Effects of Interaction of Power Converters Coupled via Power Grid: A Design-Oriented Study

Cheng Wan, Meng Huang, *Member, IEEE*, Chi K. Tse, *Fellow, IEEE*, and Xinbo Ruan, *Senior Member, IEEE*

***Abstract*—Voltage-source converters are commonly employed as rectifiers for providing a regulated dc voltage from an ac power source. In a typical microdistribution system, the power grid is nonideal and often presents itself as a voltage source with significant impedance. Thus, power converters connected to the grid interact with each other via the nonideal grid. In this paper, we study how stability can be compromised in a system of interacting grid-connected converters, which are used typically as rectifiers. Specifically, the stable operating regions in the selected parameter space may shrink when grid-connected converters interact under certain conditions. We consider the effect of both source (grid) impedance and transmission line impedance between converters, and derive bifurcation boundaries in the parameter space. A small-signal model in the *dq*-frame is adopted to analyze the interacting system using an impedance-based approach. It is shown that the system of interacting converters can become unstable. Moreover, results are presented in design-oriented forms so as to facilitate the identification of variation trends of stable operation boundaries. Experimental results verify the instability phenomenon.**

***Index Terms*—Grid-connected converters, interacting systems, power converters, stability analysis.**

I. Introduction

THREE-PHASE pulsewidth-modulated (PWM) voltage-source converters (VSCs) operating in rectifier mode have become a popular choice for ac–dc power conversion in many medium- to high-power applications. Due to the many desirable features that the VSC offers, e.g., low current harmonics, controllable power quality, and high efficiency, the VSC has been used in a variety of industrial and commercial applications, such as uninterruptible power supply systems, power supplies for telecommunication equipment, HVDC systems, distributed energy sources for renewable energy generation, battery storage systems, power conversion systems for process technology, and so on [1]. In most of these applications, the VSC does not only function as a high-performance power load to the ac power source, but also a reliable interface for many power conversion systems with the ac source.

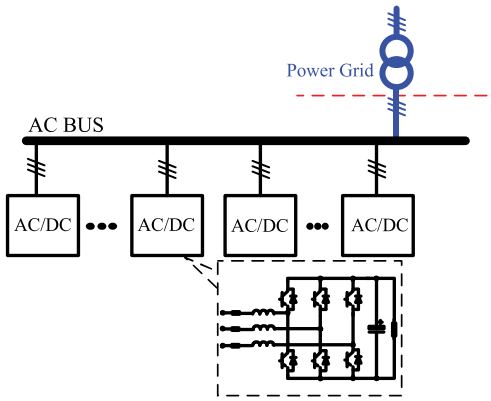

Fig. 1. Multiple VSCs connected to power grid.

As the spectrum of applications of VSCs widens, it can be appreciated that multiple VSCs may connect to the power grid at a so-called *common point of coupling* (PCC), while each VSC works under its own specific condition, as shown in the usual representation of Fig. 1 [2]. The same structure is also employed in some specific application scenarios, including aircraft power systems [3], shipboard power systems [4], microgrids [5], etc. As each converter is designed separately for its own load condition, the mutual coupling in practice via the grid may pose a stability concern as the grid is nonideal in reality and presents at the point of common coupling a significant amount of impedance, which is not always predictable. As a result, the stability of the system should be considered with the coupled system model in mind rather than the unrealistic though simple model, where each converter is assumed to behave independently.

For the purpose of illustrating the effect of mutual coupling, it suffices to consider two converters under the structure shown in Fig. 2. To maintain generality of our study, the VSCs are controlled under a typical feedback configuration that contains an outer voltage loop, which operates in conjunction with a sinusoidal PWM inner current loop for achieving a constant output dc voltage, as presented in Fig. 3. The two converters have been designed separately according to their respective application conditions. However, when they are connected to the grid, their interaction may have an impact on stability. Furthermore, in practice, the effect of transmission line impedance L_L

Manuscript received March 16, 2014; revised June 27, 2014; accepted August 12, 2014. Date of publication August 21, 2014; date of current version February 13, 2015. The work was supported in part by Hong Kong Research Grants Council under GRF Grant 5267/12E, and Hong Kong Polytechnic University Grant G-YJ62. Recommended for publication by Associate Editor Y. Sozer.

C. Wan was with the Department of Electronic and Information Engineering, Hong Kong Polytechnic University, Kowloon, Hong Kong. He is now with the State Key Laboratory of Advanced Electromagnetic Engineering and Technology, Huazhong University of Science and Technology, Wuhan 430074, China (e-mail: wchghust@gmail.com).

M. Huang was with the Department of Electronic and Information Engineering, Hong Kong Polytechnic University, Kowloon, Hong Kong. He is now with the School of Electronic Engineering, Wuhan University, Wuhan 430072, China (e-mail: meng.huang@connect.polyu.hk).

C. K. Tse is with the Department of Electronic and Information Engineering, Hong Kong Polytechnic University, Kowloon, Hong Kong (e-mail: michael.tse@polyu.edu.hk).

X. Ruan is with the College of Automation Engineering, Nanjing University of Aeronautics and Astronautics, Nanjing 210016, China (e-mail: ruanxb@nuaa.edu.cn).

Color versions of one or more of the figures in this paper are available online at http://ieeexplore.ieee.org.

Digital Object Identifier 10.1109/TPEL.2014.2349936

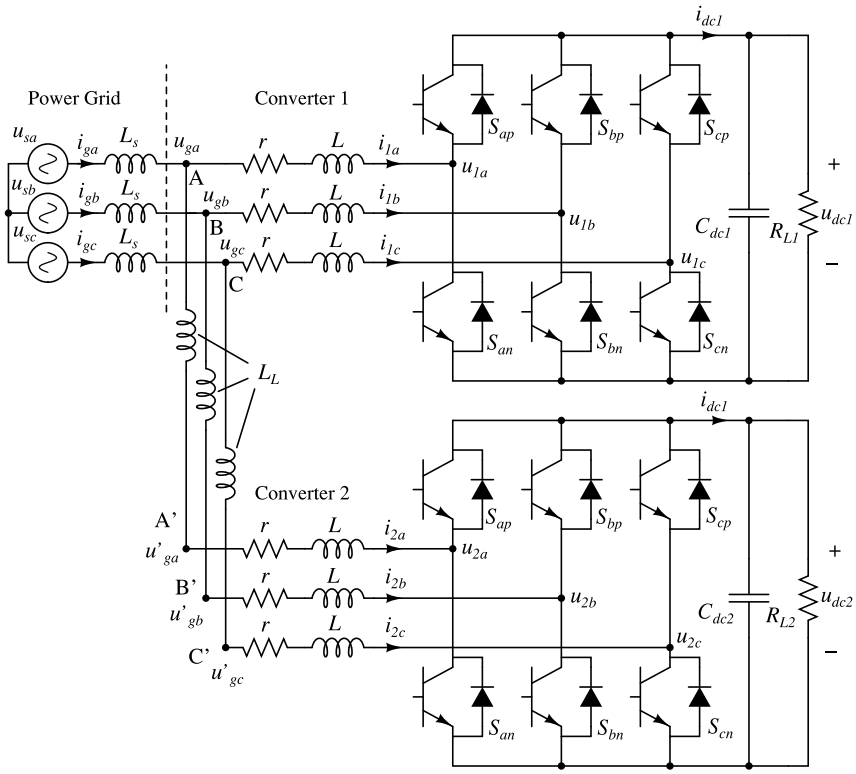

Fig. 2. Basic model of two VSCs connected to the nonideal grid.

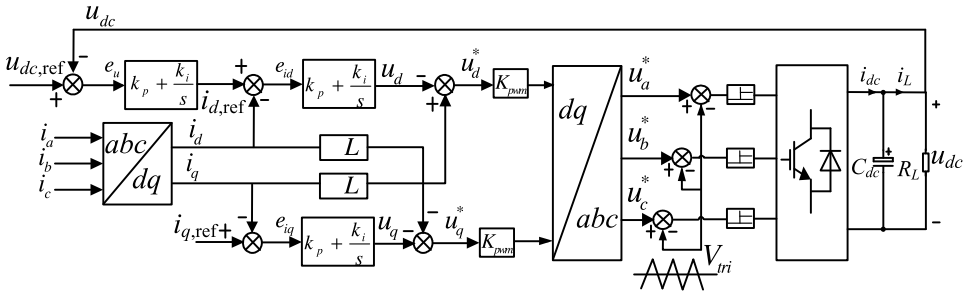

Fig. 3. Controller schematic of the three-phase VSC with filter in a rotating dq reference frame.

between converters should also be considered [6], as represented in Fig. 2.

The stability issue of grid-connected VSCs in the presence of varying grid impedance has been discussed in several prior publications. For instance, Belkhayat [7] presented an impedance-based approach to evaluate the stability of ac interfaces in the dq-frame by employing a generalized Nyquist stability criterion based on small-signal modeling, and for three-phase rectifiers, the analysis assumed an ideal power grid. The stability of grid-connected inverters and rectifiers have also been discussed by Sun [9], Burgos *et al.* [10], Belkhayat *et al.* [12], and Vesti *et al.* [11]. Moreover, a converter's impedance modeling has been studied in some detail by Harnefors *et al.* [13], Céspedes and Sun [14], [15], He *et al.* [16], and Huang *et al.* [17]. However, the key parameters of converters that would affect the system's stability significantly has rarely been discussed and identified. Furthermore, Chandrasekaran *et al.* [18], Wan *et al.* [19], and Huang *et al.* [20] have reported the effects of grid impedance on grid-connected interacting converters, but these works focused on the stability of one converter and avoided the complication of analyzing the more realistic situation where two or more converters' interact in the presence of significant grid impedance. While literature abounds with studies of three-phase rectifiers [23]–[26], in-depth study of variation of control parameters on stability of interacting three-phase rectifiers is still glaringly insufficient. Furthermore, from previous study of nonlinear behavior of power converters, some bifurcation phenomena have been observed and reported [27]–[29], which provide effective analytical tools for some in-depth study of stability of interacting converters.

TABLE I
PARAMETERS OF NONIDEAL POWER GRID

$u_{sa,sb,sc}$	f_l	L_s	L_L
110 Vrms	50 Hz	0.1–1.5 mH	0–100 μH

TABLE II
CIRCUIT PARAMETERS OF CONVERTER 1

$U_{\mathrm{dc,ref}}$	C_{dc}	L_1	R_{L1}	r	f_s
360 V	1200 μF	3 mH	30–75 Ω	0.01 Ω	10 kHz

Parameters are as Shown in Figs. 2 and 3

TABLE III
CIRCUIT PARAMETERS OF CONVERTER 2

$U_{\mathrm{dc,ref}}$	C_{dc}	L_2	R_{L2}	r	f_s
360 V	1200 μF	3 mH	30–75 Ω	0.01 Ω	10 kHz

Parameters are as Shown in Figs. 2 and 3

In this paper, we attempt to address the important issue of the effect of interaction between the grid-connected converters under nonideal power grid conditions, which has remained largely unexplored despite its practical importance. Our study will probe into the key control parameters and examine how variation of these parameters alters the stability regions under the effect of converters' interaction. Specifically, we focus on the loss of stability corresponding to emergence of a low-frequency oscillation as commonly studied under the broad class of Hopf-type bifurcation phenomena [32]. We show that the bifurcation boundaries (stability regions from an engineering viewpoint) generally shrink when converters interact via the nonideal grid. In other words, results obtained from analysis that assumes independent (uncoupled) converters under ideal grid condition, therefore, provide overoptimistic stability prediction. In Section II, we present several instability phenomena arising from converters' interaction. In Section III, in the presence and absence of transmission line impedance, a detailed stability assessment employing an impedance-based approach is presented. In Section IV, we present our results in a design-oriented format that reveals the way in which stability would be affected by variation of selected parameters, and hence, facilitates the choice of parameters for stable operation [33]. Moreover, Section V presents the observed instability phenomenon experimentally. Finally, Section VI concludes the paper.

II. GLIMPSE AT THE INSTABILITY

We begin by taking a quick glimpse at the way in which a VSC loses stability. The circuit of Fig. 2 is studied in full circuit implementation using MATALAB. The values of the circuit components used in the simulation are summarized in Tables I, II, and III. Converters 1 and 2 employ the same control method that is described in Fig. 3.

Fig. 4(a) shows stable operation of the two converters with different load conditions when separately connected to the same nonideal grids with impedance $L_s = 1.2$ mH. Thus, the converters are stable when analyzed separately. However, when the converters are connected at the same time to the nonideal grid having the same impedance at the PCC, i.e., $L_L = 0$, as shown in Fig. 2, the converters' output voltages have manifested low-frequency oscillations that are typical Hopf-type instability, as shown in Fig. 4(b). The dc voltage U_{dc} of both converters oscillate at 255 Hz around the regulated level, while all converters' parameters have remained the same as in the case of independent (uncoupled) operation. Thus, it can be inferred that the converters could interact with each other and lose stability via a Hopf-type bifurcation when the values of parameters are selected beyond a specific region in the parameter space (referred to as stability region here).

Moreover, the two converters may not be connected at the same PCC in practice. Thus, $L_L \neq 0$. When the converters are connected to the same grid at different points of coupling, the presence of nonzero transmission line impedance L_L between the two converters' connection points could affect stability, as shown in Fig. 5. We see that the two converters connected to the nonideal grid at the same PCC are originally stable, as shown in Fig. 5(a), but can become unstable when the coupling points are separated by nonzero transmission line impedance, as shown in Fig. 5(b). Thus, the converters connected to a nonideal grid can be made unstable by the presence of transmission line impedance separating the points of coupling.

III. ANALYSIS

Literature abounds with conventional methods for analyzing converter's stability [9]. For an individual grid-connected VSC, control models and their closed-loop stability analysis have been studied, employing techniques like root locus analysis and Bode diagrams. Moreover, the state-space approach is also used to determine stability in the time domain [20]. For grid-connected converters, prior studies [7], [22] have pointed out that the impedance-based approach is more advantageous and flexible. For the case of the grid-connected system under study, the impedance-based analysis is highly suitable, as will be demonstrated in the subsequent sections.

A. Basic Model: The Standalone Converter

Following the formulation of Sun [21], the three-phase VSC can be represented by an averaged model in the dq rotating coordinate. Since converters 1 and 2 share the same model, we provide, for brevity, the equations for converter 1 as follows:

$$\begin{aligned} L_1\frac{di_{1d}}{dt} &= \omega_l L_1 i_{1q} + u_{gd} - r_1 i_{1d} - u_{1d} \\ L_1\frac{di_{1q}}{dt} &= -\omega_l L_1 i_{1d} + u_{gq} - r_1 i_{1q} - u_{1q} \\ C_{\mathrm{dc1}}\frac{du_{\mathrm{dc1}}}{dt} &= \frac{3}{2}(d_{1d}i_{1d} + d_{1q}i_{1q}) - i_{o1} \end{aligned} \tag{1}$$

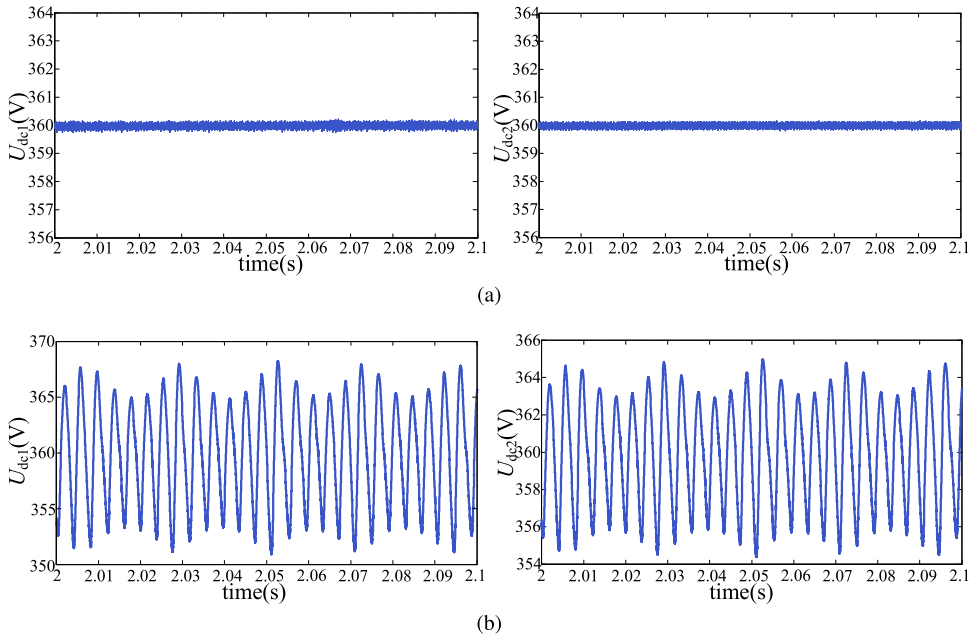

Fig. 4. Waveforms of the two converters' output voltages with $R_{L1} = 22.5\ \Omega$ and $R_{L2} = 27\ \Omega$ with the same set of control parameters $k_{vp} = 2.4, k_{vi} = 20, k_{ip} = 24, k_{ii} = 100$. (a) Two converters work independently (with no interaction) under same grid impedance $L_s = 1.2$ mH, showing stable operation; (b) two converters interact via connecting to the nonideal grid with $L_s = 1.2$ mH, showing unstable operation or Hopf-type instability.

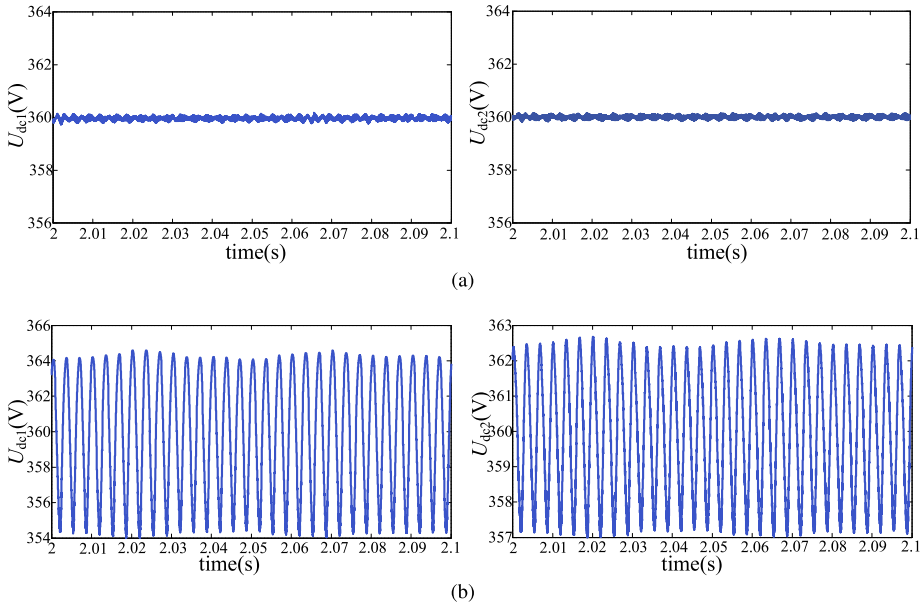

Fig. 5. Waveforms of the two converters' output voltages with $R_{L1} = 22.5\,\Omega$ and $R_{L2} = 30\,\Omega$ with the same set of control parameters $k_{vp} = 2.4, k_{vi} = 20, k_{ip} = 24, k_{ii} = 100$. (a) Two converters interact at the same PCC with $L_s = 1.2$ mH and transmission line impedance $L_L = 0$, showing stable operation; (b) two converters interact via connecting to different points of coupling with $L_s = 1.2$ mH and transmission line impedance $L_L = 70\,\mu$H, showing unstable operation or Hopf-type instability.

where subscript 1 denotes converter 1 (likewise, subscript 2 denotes converter 2 in the subsequent analysis); $\omega_l = 2\pi f_l$; $d_{1d} = u_{1d}/u_{\mathrm{dc1}}$ and $d_{1q} = u_{1q}/u_{\mathrm{dc1}}$ are the duty cycles; i_{1d} and i_{1q} are the input currents of converter 1 in the dq-frame; u_{gd} and u_{gq} are the voltages at the PCC; u_{1d} and u_{1q} are the leg voltages in the dq-frame; and i_{o1} is the load current. For simplicity, we ignore the inductor resistance r in the following analysis.

From (1), we can obtain the small-signal representation via the usual linearization procedure, i.e.

$$\frac{d\hat{i}_{1d}}{dt} = \omega_l \hat{i}_{1q} - \frac{\hat{u}_{\mathrm{dc1}} D_{1d} + \hat{d}_{1d} U_{\mathrm{dc1}}}{L_1} + \frac{\hat{u}_{gd}}{L_1}$$
$$\frac{d\hat{i}_{1q}}{dt} = -\omega_l \hat{i}_{1d} - \frac{\hat{u}_{\mathrm{dc1}} D_{1q} + \hat{d}_{1q} U_{\mathrm{dc1}}}{L_1} + \frac{\hat{u}_{gq}}{L_1}$$

$$\frac{d\hat{u}_{\rm dc1}}{dt} = \frac{3}{2C_{\rm dc1}}(D_{1d}\hat{i}_{1d} + D_{1q}\hat{i}_{1q} + \hat{d}_{1d}I_{1d} + \hat{d}_{1q}I_{1q}) - \frac{\hat{i}_{o1}}{C_{\rm dc1}} \quad (2)$$

where $D_{1d}, D_{1q}, I_{1d}, I_{1q}$, and $U_{\rm dc1}$ are the system's steady-state values, which are given by

$$D_{1d} = \frac{U_{sd}}{U_{\rm dc1}},\ D_{1q} = \frac{-\omega_l L_1 I_{1d}}{U_{\rm dc1}},\ I_{1d} = \frac{2U_{\rm dc1}^2}{3R_{L1}U_{sd}}$$
$$I_{1q} = I_{1q-\rm ref},\ \text{and}\ U_{\rm dc1} = U_{\rm dc1-ref}. \quad (3)$$

Here, the state variables are $\hat{i}_{1d}$, $\hat{i}_{1q}$, and $\hat{u}_{\rm dc1}$; the controlled variables are $\hat{d}_{1d}$ and $\hat{d}_{1q}$; and the disturbances are $\hat{u}_{sd}$, $\hat{u}_{sq}$, and $\hat{i}_o$. The small-signal model can be represented in the s-domain as follows:

$$s\begin{bmatrix} I_{1d}(s) \\ I_{1q}(s) \\ U_{\rm dc1}(s) \end{bmatrix} = \begin{bmatrix} 0 & \omega_l & -\frac{D_{1d}}{L_1} \\ -\omega_l & 0 & -\frac{D_{1q}}{L_1} \\ \frac{3D_{1d}}{2C_{\rm dc1}} & \frac{3D_{1q}}{2C_{\rm dc1}} & 0 \end{bmatrix}\begin{bmatrix} I_{1d}(s) \\ I_{1q}(s) \\ U_{\rm dc1}(s) \end{bmatrix} + \begin{bmatrix} -\frac{U_{\rm dc1}}{L_1} & 0 \\ 0 & -\frac{U_{\rm dc1}}{L_1} \\ \frac{3I_{1d}}{2C_{\rm dc1}} & \frac{3I_{1q}}{2C_{\rm dc1}} \end{bmatrix}\begin{bmatrix} D_{1d}(s) \\ D_{1q}(s) \end{bmatrix} + \begin{bmatrix} \frac{1}{L_1} & 0 & 0 \\ 0 & \frac{1}{L_1} & 0 \\ 0 & 0 & -\frac{1}{C_{\rm dc1}} \end{bmatrix}\begin{bmatrix} U_{gd}(s) \\ U_{gq}(s) \\ I_{o1}(s) \end{bmatrix}. \quad (4)$$

The typical control configuration for VSCs consists of two loops, as shown in Fig. 3. The inner loop is used to minimize the errors between the reference signals $(i_{d\rm ref}, i_{q\rm ref})$ and the sensed currents (i_d, i_q), and the outer voltage loop is responsible for minimizing the error between $u_{\rm dc-ref}$ and $u_{\rm dc}$. The duty cycles can be derived as

$$\begin{bmatrix} D_{1d}(s) \\ D_{1q}(s) \end{bmatrix} = \begin{bmatrix} \frac{G_{i1}}{U_{\rm dc1}} & \frac{\omega_l L_1}{U_{\rm dc1}} & \frac{G_{v1}G_{i1}}{U_{\rm dc1}} \\ -\frac{\omega_l L_1}{U_{\rm dc1}} & \frac{G_{i1}}{U_{\rm dc1}} & 0 \end{bmatrix}\begin{bmatrix} I_{1d}(s) \\ I_{1q}(s) \\ U_{\rm dc1}(s) \end{bmatrix} \quad (5)$$

where $G_{v1} = k_{vp} + k_{vi}/s$ and $G_{i1} = k_{ip} + k_{ii}/s$. From (4) and (5), we obtain the state-space representation of the closed-loop system as

$$s\begin{bmatrix} I_{1d}(s) \\ I_{1q}(s) \\ U_{\rm dc1}(s) \end{bmatrix} = A\begin{bmatrix} I_{1d}(s) \\ I_{1q}(s) \\ U_{\rm dc1}(s) \end{bmatrix} + B\begin{bmatrix} U_{gd}(s) \\ U_{gq}(s) \\ I_{o1}(s) \end{bmatrix} \quad (6)$$

where $A =$

$$\begin{bmatrix} -\frac{G_{i1}}{L_1} & 0 & -\frac{D_{1d}}{L_1} - \frac{G_{v1}G_{i1}}{U_{\rm dc1}} \\ 0 & -\frac{G_{i1}}{L_1} & -\frac{D_{1q}}{L_1} \\ \frac{3D_{1d}}{2C_{\rm dc1}} + \frac{3G_{i1}I_{1d}}{2C_{\rm dc1}U_{\rm dc1}} & \frac{3D_{1q}}{2C_{\rm dc1}} + \frac{3I_{1d}\omega_l L_1}{2C_{\rm dc1}U_{\rm dc1}} & \frac{3I_{d1}G_{v1}G_{i1}}{2C_{\rm dc1}U_{\rm dc1}} \end{bmatrix}$$

and

$$B = \begin{bmatrix} \frac{1}{L_1} & 0 & 0 \\ 0 & \frac{1}{L_1} & 0 \\ 0 & 0 & -\frac{1}{C_{\rm dc1}} \end{bmatrix}. \quad (7)$$

For brevity of presentation, we define

$$I_1 = \begin{bmatrix} I_{1d}(s) \\ I_{1q}(s) \end{bmatrix},\ U_g = \begin{bmatrix} U_{gd}(s) \\ U_{gq}(s) \end{bmatrix},\ Y_{1i} = \begin{bmatrix} \frac{1}{L_1} & 0 \\ 0 & \frac{1}{L_1} \end{bmatrix}$$

$$G_{1id} = \begin{bmatrix} -\frac{G_{i1}}{L_1} & 0 \\ 0 & -\frac{G_{i1}}{L_1} \end{bmatrix},\ A_{1i} = \begin{bmatrix} -\frac{D_{1d}}{L_1} - \frac{G_{v1}G_{i1}}{U_{\rm dc1}} \\ -\frac{D_{1q}}{L_1} \end{bmatrix}$$

$$A_{1v} = \begin{bmatrix} \frac{3D_{1d}}{2C_{\rm dc1}} + \frac{3G_{i1}I_{1d}}{2C_{\rm dc1}U_{\rm dc1}} & \frac{3D_{1q}}{2C_{\rm dc1}} + \frac{3I_{1d}\omega_l L_1}{2C_{\rm dc1}U_{\rm dc1}} \end{bmatrix}$$

$$T(s) = \begin{bmatrix} G_{1id} & A_{1i} \\ A_{1v} & Z_1 \end{bmatrix},\ Z_{1o} = -\frac{1}{C_{\rm dc1}},\ Z_1 = \frac{3I_{d1}G_{v1}G_{i1}}{2C_{\rm dc1}U_{\rm dc1}}.$$

The impedance function of the closed-loop system can be written as follows:

$$\begin{bmatrix} I_1 \\ U_{\rm dc1} \end{bmatrix} = (s\mathbf{1} - T(s))^{-1}\begin{bmatrix} Y_{1i} & O \\ O & Z_{1o} \end{bmatrix}\begin{bmatrix} U_g \\ I_{o1} \end{bmatrix}. \quad (8)$$

where $\mathbf{1}$ is the unit matrix. Therefore, the characteristic polynomial that determines the stability of the closed-loop system can be found as

$$\Phi_{CL}(s) = \det(s\mathbf{1} - T(s)). \quad (9)$$

Thus, we can assess the stability of the system by inspecting the roots of $\Phi_{CL}(s) = 0$, i.e., eigenvalues of $T(s)$. Stability requires that all eigenvalues have negative real parts. Putting the parameter values in (9), we can compute the eigenvalues as given in Table IV, which indicate stable operation of the uncoupled converters.

TABLE IV
EIGENVALUES OF THE UNCOUPLED CONVERTERS (INDEPENDENTLY OPERATED)

System	Eigenvalues	Stability
Converter 1	$-1524.885 \pm j2889.817$, -4.168, -4.199, -7995.83, -8.029	Stable
Converter 2	$-1936.866 \pm j2622.119$, -4.168, -4.199, -7995.83, -8.067	Stable

B. Interacting Converters in the Absence of Transmission Line Impedance

The foregoing section derives the conventional converter's closed-loop model and assesses the stability of the converters when working independently (uncoupled). In this section, the converters are connected to the power grid at a common coupling point (i.e., $L_L = 0$), and thus, interact with each other. As the

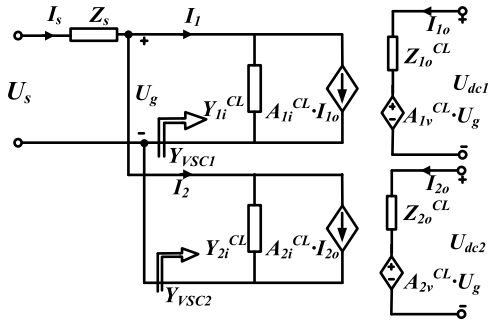

Fig. 6. Impedance model of the system of interacting converters in dq-frame.

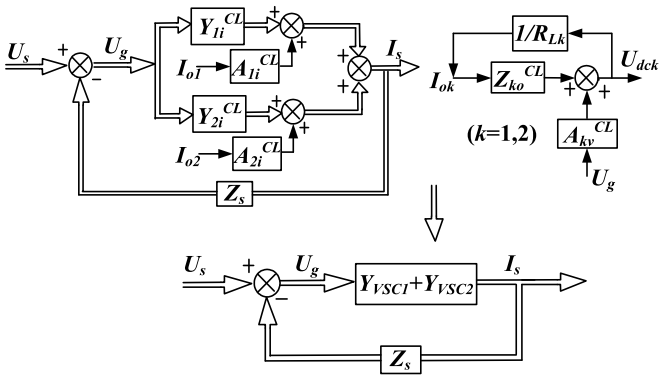

Fig. 7. Block diagram of the impedance model of the system of interacting converters in dq-frame.

two converters have identical control loops, from (8), we can derive the converters' impedance as

$$\begin{bmatrix} I_k \\ U_{\mathrm{dc}k} \end{bmatrix} = \begin{bmatrix} Y_{ki}^{CL} & A_{ki}^{CL} \\ A_{kv}^{CL} & Z_{ko}^{CL} \end{bmatrix} \begin{bmatrix} U_g \\ I_{ok} \end{bmatrix}, (k=1,2)$$

$$\begin{bmatrix} Y_{ki}^{CL} & A_{ki}^{CL} \\ A_{kv}^{CL} & Z_{ko}^{CL} \end{bmatrix} = (s\mathbf{1} - T(s))^{-1} \begin{bmatrix} Y_{ki} & O \\ O & Z_{ko} \end{bmatrix}. \quad (10)$$

Combining (10) and $I_o = U_{\mathrm{dc}}/R_L$, we obtain the input admittance of each converter as seen at the coupling point as well as the overall input admittance, i.e.

$$\begin{aligned} Y_{\mathrm{VSC}k} &= Y_{ki}^{CL} + [R_{Lk} - Z_{ko}^{CL}]^{-1} A_{ki}^{CL} A_{kv}^{CL}, (k=1,2) \\ Y(s) &= Y_{\mathrm{VSC1}} + Y_{\mathrm{VSC2}} \end{aligned} \quad (11)$$

where $Y_{\mathrm{VSC}k}$ $(k=1,2)$ is the converter's input admittance and $Y(s)$ is the total input admittance of the two converters.

In a likewise manner, the grid impedance can be found from

$$Z_s I_s = U_s - U_g \quad (12)$$

where

$$I_s = \begin{bmatrix} I_{sd} \\ I_{sq} \end{bmatrix}, U_s = \begin{bmatrix} U_{sd} \\ U_{sq} \end{bmatrix}, Z_s = \begin{bmatrix} L_s s & -\omega_l L_s \\ \omega_l L_s & L_s s \end{bmatrix}. \quad (13)$$

Thus, the system's impedance can be considered in the usual Thévenin form, as shown in Fig. 6.

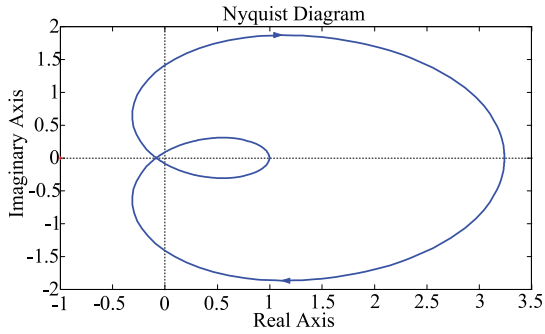

Fig. 8. Nyquist diagram of the system of interacting converters.

TABLE V
EIGENVALUES OF THE SYSTEM OF INTERACTING CONVERTERS

System	Eigenvalues	Stability
Connected system	$61.616 \pm j2439.676$, $-1749.02 \pm j2739.079$, -4433.38, $-4.19 \pm j0.011$, -4.168, -4.199, -8.03, -8.06, -7995.83	Unstable

Based on this small-signal model, the current I_s from power grid to the coupled converters is

$$I_s = [\mathbf{1} + Y(s)Z_s]^{-1} Y(s) U_s. \quad (14)$$

Since the converters are stable when operating independently, both U_s and $Y(s)$ are stable and the stability of the connected system can be assessed by applying Nyquist criterion [8] to

$$H(s) = [\mathbf{1} + Y(s)Z_s]^{-1}. \quad (15)$$

The Nyquist plot of $\det[\mathbf{1} + Y(s)Z_s]$, for the purpose of determining stability of the closed-loop system [30], is given in Fig. 8, which shows encirclement of the origin, and hence, asserts that the system is unstable. Numerical calculations of the poles of the closed-loop system also indicate unstable operation, as shown in Table V. This result is in full agreement with the simulations presented earlier.

For a general system with multiconverters connected to a nonideal power grid at the same PCC as shown in Fig. 1, we can track the trajectory to determine the overall system's stability. The total input admittance of the connected system is $Y_{\mathrm{VSC}} = Y_{\mathrm{VSC1}} + Y_{\mathrm{VSC2}} + Y_{\mathrm{VSC3}} + \cdots + Y_{\mathrm{VSC}n}$, and the impedance in dq-frame can be obtained as shown in Fig. 9. The stability can be assessed by examining the root locus of $\det[\mathbf{1} + Y_{\mathrm{VSC}} Z_s] = 0$.

C. Interacting Converters in the Presence of Transmission Line Impedance

When the two converters are connected to a nonideal power grid at different points separated by an impedance (i.e., $L_L > 0$ in Fig. 2), stability of the system can be affected, as observed previously in Section II. Using the same impedance-based approach, we can readily find the Thévenin equivalent circuit of

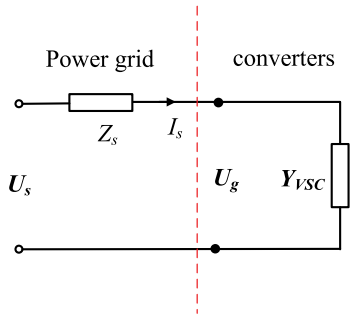

Fig. 9. Thévenin equivalent circuit of multiple VSCs connected to a nonideal power grid at the same coupling point.

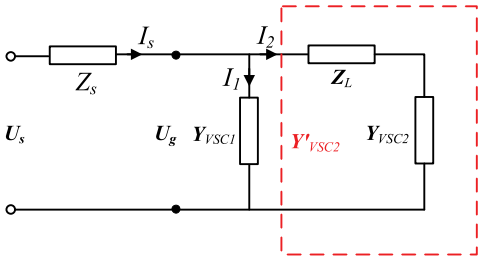

Fig. 10. Impedance model of the system with transmission line impedance in dq-frame.

TABLE VI
EIGENVALUES OF THE SYSTEM OF INTERACTING CONVERTERS WITH NONZERO TRANSMISSION LINE IMPEDANCE

L_L	Eigenvalues	Stability
40 μH	$-4.679 \pm j2447.89$, $-1853.05 \pm j2633.7$, -4417.128, -4.16, -4.169, -4.199, -4.224, -8.027, -8.084, -7943.28	Stable
50 μH	$-1.22 \pm j2446.77$, $-1847.96 \pm j2634.06$, -4413.0, -4.16, -4.169, -4.199, -4.224, -8.027, -8.084, -7930.39	Stable
60 μH	$2.23 \pm j2445.63$, $-1842.92 \pm j2634.42$, -4408.86, -4.16, -4.169, -4.199, -4.224, -8.027, -8.084, -7917.59	Unstable
70 μH	$5.68 \pm j2444.48$, $-1837.93 \pm j2634.75$, -4404.71, -4.16, -4.169, -4.199, -4.224, -8.027, -8.084, -7904.89	Unstable

the system in the presence of transmission line impedance in the dq-coordinate, as shown in Fig. 10. Here, Z_L is the impedance of the transmission line. Therefore, to ensure stability of the system, Y_{VSC1} and Y'_{VSC2} should be stable, where Y'_{VSC2} is the combined admittance of converter 2 and the transmission line. From Kirchhoff's laws, Y'_{VSC2} can be found as

$$Y'_{\mathrm{VSC2}} = [\mathbf{1} + Y_{\mathrm{VSC2}} Z_L]^{-1} Y_{\mathrm{VSC2}} \tag{16}$$

where

$$Z_L = \begin{bmatrix} sL_L & -\omega_l L_L \\ \omega_l L_L & sL_L \end{bmatrix}. \tag{17}$$

Similarly, if Y_{VSC2} and $[\mathbf{1} + Y_{\mathrm{VSC2}} Z_L]^{-1}$ are stable, so is Y'_{VSC2}. Thus, the system can be regarded as two admittances Y_{VSC1} and Y'_{VSC2} connected to the grid. The total admittance is $Y(s) = Y_{\mathrm{VSC1}} + Y'_{\mathrm{VSC2}}$, and using (14) again, we examine the roots of $\det[\mathbf{1} + Y(s)Z_s] = 0$ for stability assessment. Table VI presents the system's eigenvalues with different values of transmission line impedance. It can be concluded that transmission line impedance destabilizes the system, and as the transmission line impedance gets larger, the interacting converters becomes more prone to instability.

The aforementioned analysis clearly shows that the interacting converters can be unstable, while the individual separately operated converters are stable, and that the interacting converters can also become unstable in the presence of transmission line impedance between the points of coupling.

IV. Design-Oriented Results and Verification

The foregoing analysis provides a precise tool for determining the system's stability using interface impedance. However, for engineering design purposes, it is more useful to identify the system parameters and their variation trends that have significant impact on the stable region of operation [31], [33]. In this section, we derive stability boundaries using the foregoing analysis and present them in design-oriented forms. Results from simulations of the actual switching circuits will also be presented for comparison and verification.

Relevant to our present study is the region of stable operation bounded by the bifurcation boundary corresponding to the loss of stability via a Hopf-type bifurcation (practically known as low-frequency oscillation). For the system of two converters connected to a nonideal power grid, we focus on the following parameters:

1) the grid impedance L_s;
2) the transmission line impedance L_L;
3) the dc gains of the two converters' voltage loop k_{vp1}, k_{vp2};
4) the converters' load resistance R_{L1}, R_{L2};
5) the dc-link capacitance $C_{\mathrm{dc1}}, C_{\mathrm{dc2}}$.

Moreover, for the purpose of comparison, the stability regions of converters coupled via the power grid and those of the independently operating (uncoupled) converters are presented. Our results are generated from simulations of the complete switching model, which provides viable verification of the actual physical system.

In the sequel, we will present a series of design-oriented stability charts, which are computed from the analysis of Section II and also from full circuit simulations. Each chart contains two sets of stability boundaries, shown in red and blue, corresponding to two specific parameter values as labeled in the chart. In each chart, for the red or blue set of boundaries, the parameter plane is divided into regions I, II, and III:

1) region I (stable) is the parameter region, where the system is stable for both cases of independently operated converters and grid-coupled converters;
2) region II (intermediate) is the parameter region, where the independently operated converters are stable, but the system of grid-coupled converters is unstable;
3) region III (unstable) is the parameter region, where the system is unstable for both cases of independently operated converters and grid-coupled converters.

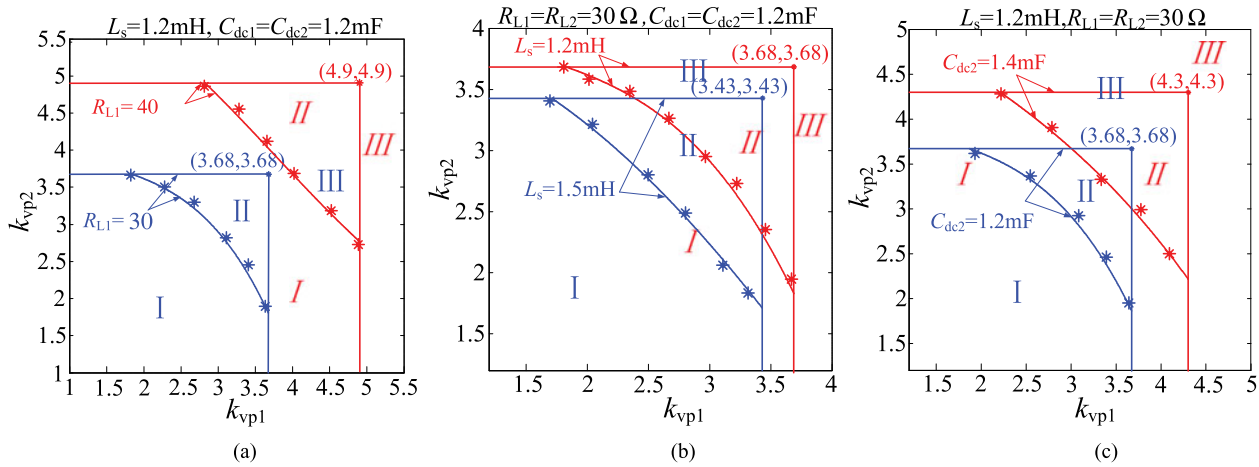

Fig. 11. Stability boundaries on the 2-dim plane of dc gains, i.e., k_{vp1} versus k_{vp2}, with (a) variation of converter 1's dc load R_{L1} with $R_{L2} = R_{L1}$; (b) variation of grid impedance L_s with $R_{L1} = R_{L2} = 30\,\Omega$; (c) variation of converter 2's dc-link capacitor $C_{\rm dc2}$ with $C_{\rm dc1} = C_{\rm dc2}$. Points $(*)$ are calculated from analysis of Section III and solid curves are from full circuit simulations.

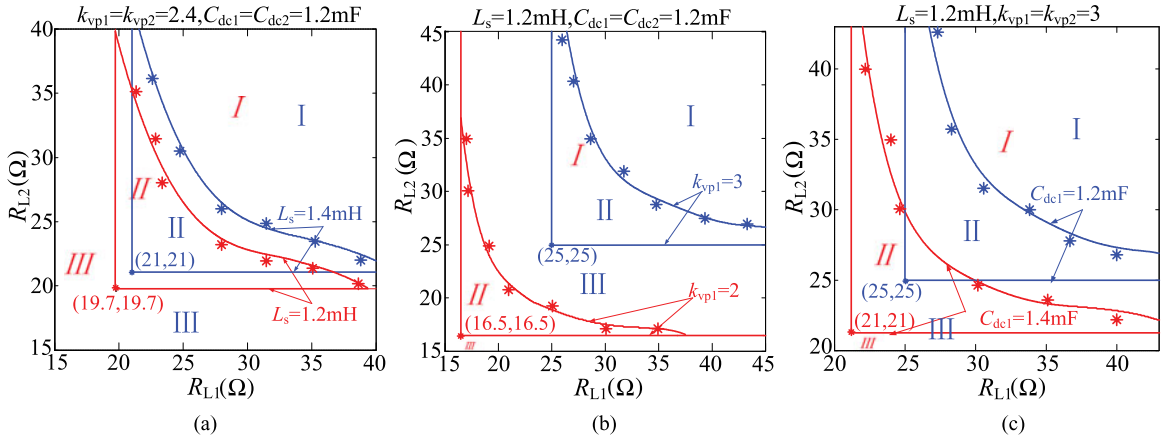

Fig. 12. Stability boundaries on the 2-dim plane of load resistances, i.e., R_{L1} versus R_{L2}, with (a) variation of grid impedance L_s with $k_{vp1} = k_{vp2} = 2.4$; (b) variation of dc gain of converter's voltage loop with $k_{vp1} = k_{vp2}$; (c) variation of the dc-link capacitor with $C_{\rm dc1} = C_{\rm dc2}$. Points $(*)$ are calculated from analysis of Section III and solid curves are from full circuit simulations.

Thus, the boundary separating regions I and II is the bifurcation boundary or stability threshold for the system of coupled converters, and the boundary separating regions II and III is the bifurcation boundary for the independently operated converter. In each chart, analytically calculated stability boundaries are plotted in asterisk $(*)$, and the corresponding full circuit simulated boundaries are shown in solid curves.

The dc gains of voltage loop k_{vp1}, k_{vp2} are the key parameters that affect stability with respect to Hopf bifurcation. Since the inner current loop gain is usually chosen to be sufficiently high to ensure that the current tracks the reference closely, we will ignore the inner-loop gain in our study. For the system of converters connected at the same PCC, the stability regions in the k_{vp1}–k_{vp2} plane is shown in Fig. 11, for both the uncoupled and coupled systems for different values of dc loads, grid impedance, and dc-link capacitors. These charts reveal how variation of these parameters would affect the stability regions, and specifically we see that the stable operating regions are reduced when either dc load current, line impedance, or dc-link capacitor is increased.

The dc load resistance of the converters can affect stability, as shown in the design-oriented charts of Fig. 12. From the charts presented in Fig. 12, when one converter is more heavily loaded, the system moves closer to the boundary of instability. Moreover, we observe that the region of stability shrinks when the converters are coupled via the nonideal grid.

The converter's dc-link capacitor is another key parameter affecting stability. As shown in Fig. 13, one converter should increase its dc-link capacitor value to ensure stability if the other converter's dc-link capacitor value decreases. Moreover, under different power, control, and grid impedance conditions, the region of stability is reduced when the converters are connected to the grid.

When the converters are connected to a nonideal power grid at different coupling points, the presence of transmission line impedance affects the stability of the system, as shown in Fig. 14. It could be observed that the presence of transmission line impedance would shrink the converters' stability region.

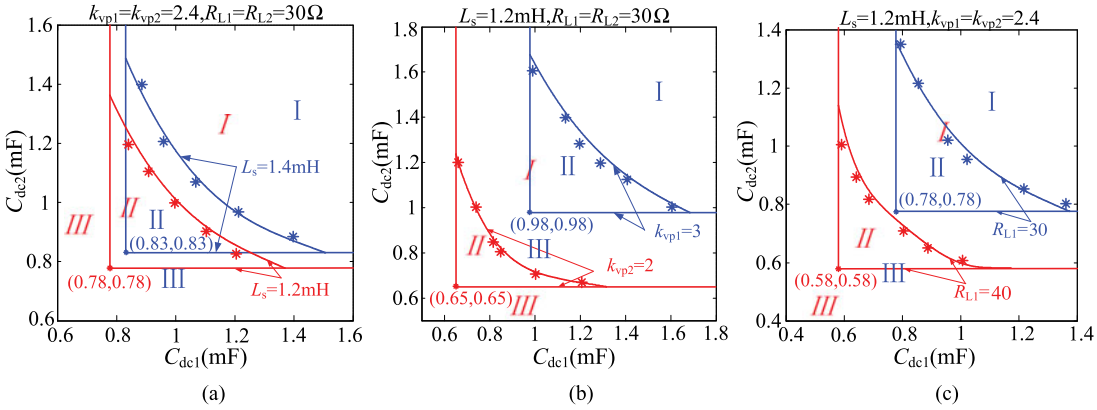

Fig. 13. Stability boundaries on the 2-D plane of dc-link capacitors, i.e., $C_{\mathrm{dc}1}$ versus $C_{\mathrm{dc}2}$, with (a) variation of grid impedance L_s with $k_{vp1} = k_{vp2} = 2.4$; (b) variation of dc gain of converter's voltage loop with $k_{vp1} = k_{vp2}$; (c) variation of converter 1's dc load R_{L1} with $R_{L2} = R_{L1}$. Points ($*$) are calculated from analysis of Section III and solid curves are from full circuit simulations.

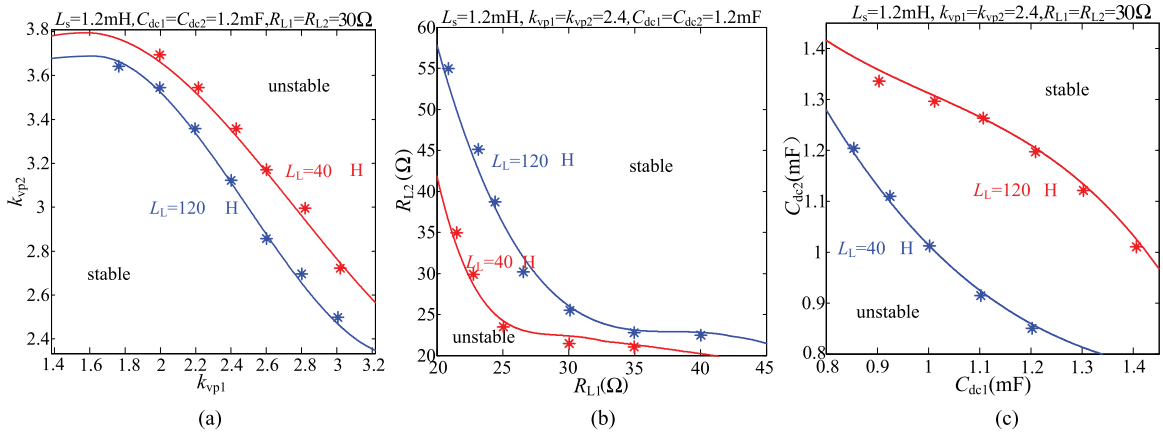

Fig. 14. Effect of varying L_L on the stability boundaries: (a) k_{vp1} versus k_{vp2} plane; (b) R_{L1} versus R_{L2} plane; (c) $C_{\mathrm{dc}1}$ versus $C_{\mathrm{dc}2}$ plane. Points ($*$) are calculated from analysis of Section III and solid curves are from full circuit simulations.

From the charts presented previously, we see that the analytically computed boundaries are in perfect agreement with the full circuit simulated results. The effects of different parameters on the overall system stability can be summarized qualitatively in Table VII. Specifically, the system would alter the stability margin when parameters vary. In the table, the "+" and "−" signs indicate increasing and decreasing values of the parameters, respectively. Correspondingly, the sign "↑" means enlarging the overall system stability margin, whereas "↓" refers to reducing the stability margin. For instance, when the load decreases (−), the overall system stability region shrinks (↓), and vice versa.

From Table VII, we see that the stability margin would enlarge when the values of -link capacitor (C_{dc}) and the converter's load (R_L) increase. On the contrary, the stability margin would shrink when the dc gain of voltage loop (k_{vp}), grid impedance (L_s), and transmission line impedance (L_L) increase. To probe further, we perform simulation to examine the variation of the stability margin when two key parameters are varied at the same time. Here, we consider varying two parameters, which have opposite effects on the stability margin when varied separately. As shown in Table VIII, the stability margin may change in different ways for different pairs of varying parameters.

TABLE VII
EFFECTS OF VARYING SYSTEM'S PARAMETERS ON STABILITY REGIONS

Parameters	Variation	Stability Margin
DC gain of voltage loop	− +	↑ ↓
DC-link capacitor	− +	↓ ↑
Converter's load	− +	↓ ↑
Grid impedance	− +	↑ ↓
Transmission line impedance	− +	↑ ↓

The "+" and "−" signs indicate increasing and decreasing values of the parameters, respectively. Correspondingly, "↑" means enlarging the overall system stability margin and "↓" refers to shrinking of the stability region.

V. EXPERIMENTAL VERIFICATION

The aim of this section is to verify the instability phenomenon observed in the previous sections. Two three-phase converters rated at 2 and 4 kW have been constructed in the laboratory. The control strategy of two converters is the same, as shown

TABLE VIII
EFFECTS OF VARYING TWO PARAMETERS ON STABILITY REGIONS

Parameters	Stability Margin
$C_{\rm dc}$, k_{vp}	↓
$C_{\rm dc}$, L_s	↑
$C_{\rm dc}$, L_L	↑
R_L , k_{vp}	↓
R_L , L_s	↑
R_L , L_L	↑

The two parameters, when increased separately, have opposite effects on stability margin. The parameter increments are 50% of their design values. The signs "↑" and "↓" denote widening and shrinking of the stability margin.

TABLE IX
CIRCUIT COMPONENTS VALUES FOR THE NONIDEAL POWER GRID

Parameters	Values
$u_{sa,sb,sc}$	110 Vrms
L_s	1.2 mH
L_L	180 μH
f_l	50 Hz

TABLE X
CIRCUIT COMPONENTS VALUES OF THE TWO EXPERIMENTAL VSCS

Parameters	Values of VSC1	Values of VSC2
$U_{\rm dc,ref}$	360 V	360 V
$C_{\rm dc}$	1000 μF	1000 μF
L	3 mH	3 mH
f_s	10 kHz	10 kHz
R_L	37 Ω	72 Ω

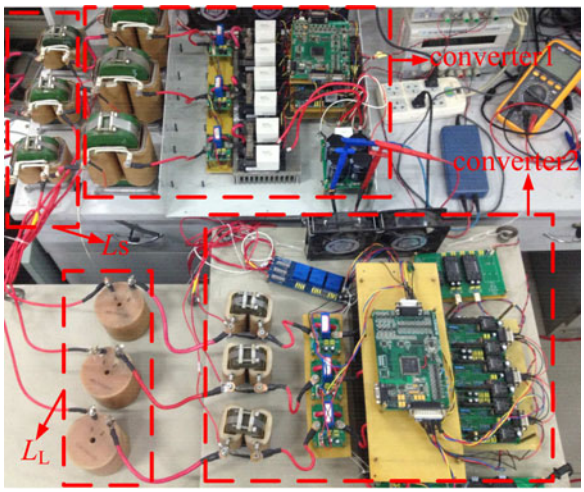

Fig. 15. Experimental circuits of two coupled power converters.

in Fig. 3, which has been realized on a DSP board. Also, the insulated-gate bipolar transistors have been applied in the converters. The grid's parameters and converters' parameters are given in Tables IX and X, respectively, which are consistent with the simulation parameters. The experimental platform is shown in Fig. 15.

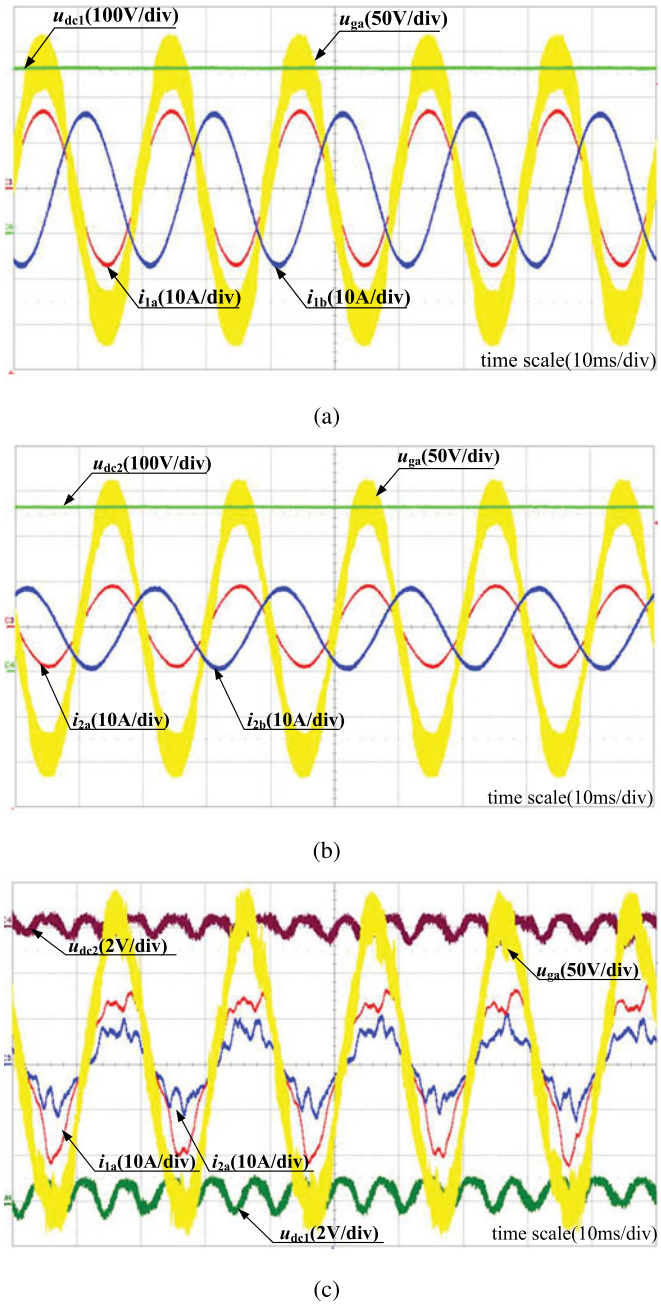

Fig. 16. Waveforms of two converters connected to a nonideal power grid with no transmission line impedance. (a) Waveforms of converter 1's line currents i_{1a} , i_{1b}, dc voltage $u_{\rm dc1}$ and PCC voltage u_{sa} when connected to the grid independently, showing stable operation. (b) Waveforms of converter 2's line currents i_{2a} , i_{2b}, dc voltage $u_{\rm dc2}$ and PCC voltage u_{sa} when connected to the grid independently, showing stable operation. (c) Waveforms of two converters' line currents i_{1a} , i_{2a}, dc voltages $u_{\rm dc1}$, $u_{\rm dc2}$, PCC line voltage u_{sa} when connected to the same grid with the same converters' parameters, showing unstable operation or low-frequency Hopf-type bifurcation.

As shown in Figs. 16(a) and (b), the two three-phase balanced converters are stable at the rated power levels when they are working independently, i.e., the grid being an ideal voltage source behind an impedance. With the same converters' parameters, when the two converters are coupled through connecting to the same nonideal power grid, both converters become unstable and exhibit Hopf bifurcation, as shown in Fig. 16(c).

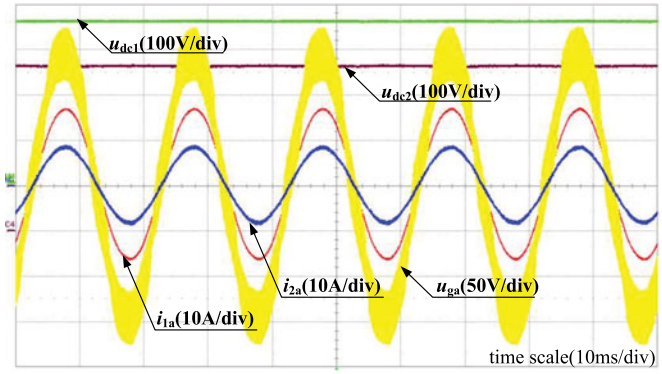

(a)

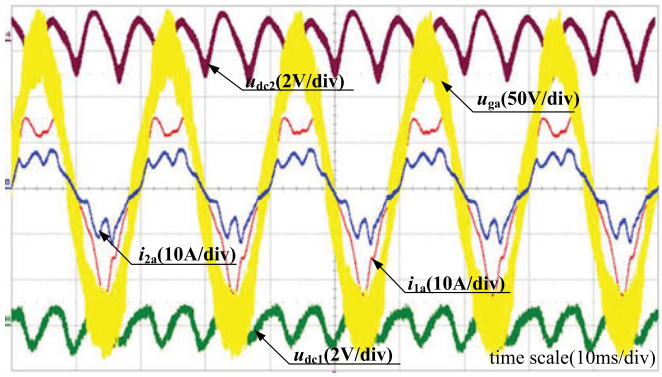

(b)

Fig. 17. Waveforms of two converters coupled via the nonideal grid. (a) Waveforms of two converters' line currents i_{1a}, i_{1b}, dc voltage $u_{\rm dc1}$, $u_{\rm dc2}$, PCC line voltage u_{sa} when coupled to the same grid with transmission line impedance $L_L = 0$, showing stable operation. (b) Waveforms of two converters' line currents i_{1a}, i_{1b}, dc voltage $u_{\rm dc1}$, $u_{\rm dc2}$, PCC line voltage u_{sa} when coupled to the same grid with transmission line impedance $L_L = 180\,\mu$H, showing unstable operation or low-frequency Hopf-type bifurcation.

The two converters exhibit low-frequency oscillation in the dc output voltages with very significant amount of low-frequency harmonics in the input line currents. This result is in perfect agreement with the simulation results shown earlier in Fig. 4. It can be observed that the oscillation frequency of the dc voltage is nearly 150 Hz. This result verifies that the two converters could interact with each other, resulting in loss of stability via Hopf bifurcation, although they are shown to be stable when they are independently operated.

Varying the control parameters, we observe that the two grid-connected converters are stable with transmission line impedance $L_L = 0$, as shown in Fig. 17(a). However, by increasing the transmission line impedance to a high value $L_L = 180\,\mu H$, which is practical [6], both converters lose stability via Hopf bifurcation, as shown in Fig. 17(b). Low-frequency oscillation in the dc voltage and a large amount of low-frequency harmonics on the line current can be clearly seen. This result clearly verifies the analytical result reported in the foregoing sections.

VI. Conclusion

Three-phase VSCs connected to a nonideal power grid are studied in this paper. The emphasis is on the coupling of two or more converters via the grid and how the resulting interaction may affect stability of the overall system. It should be readily appreciated that the method presented in this paper is applicable to three-phase grid-connected inverters. This study is important as converters are increasingly being deployed for applications involving power conversion functions that require interfacing with power grid, which is often nonideal. The significant impedance present in the grid poses an issue deserving attention as converters' stability is no longer a standalone problem. Through mutual interaction, converters become more prone to instability under certain conditions. This paper points out that the overall system stability should be reconsidered in the light of a more complete model that takes into account the interaction of converters connected to the grid at a common point of coupling or different points of coupling. Analysis has been developed using the impedance approach, and stability boundaries are derived in various parameter planes. Findings reported in this paper would facilitate engineers in making design choices related to the selection of parameter values that would guarantee stability in a sufficiently wide parameter range.

References

[1] S. Sanjuan, "*Voltage oriented control of three-phase boost PWM converters*," Master of Engineering thesis, Chalmers Univ. Technology, Göteborg, Sweden, 2010.

[2] X. F. Wang, J. M. Guerrero, Z. Chen, and F. Blaabjerg, "Distributed energy resources in grid interactive AC microgrids,"*Proc. IEEE Int. Symp. Power Electron. Distrib. Generation Syst.*, Heifei, China, 2010, pp. 806–812.

[3] K.-N. Areerak, S. V. bozhko, G. M. Asher, and D. W. P. Thomas, "Stability study for a hybrid ac-dc more-electric aircraft power system," *IEEE Trans. Aerosp. Electron. Syst.*, vol. 48, no. 1, pp. 329–347, Jan. 2012.

[4] J. G. Ciezki and R. W. Ashton, "Selection and stability issues associated with a navy shipboard dc zonal electric distribution system," *IEEE Trans. Power Del.*, vol. 15, no. 2, pp. 665–669, Apr. 2000.

[5] D. P. Ariyasinghe, and D. M. Vilathgamuwa, "Stability analysis of microgrids with constant power loads," in *Proc. IEEE Int. Conf. Sustainable Energy Technol.*, 2008, pp. 279–284.

[6] Y.-S. Kim and J.-C. Kim, "Characteristic impedance in low-voltage distribution systems for power line communication," *KIEE J. Electr. Eng. Technol*, vol. 2, no. 1, pp. 29–34, 2007.

[7] M. Belkhayat, *Stability Criteria for AC Power Systems with Regulated Loads*, Ph.D. dissertation, , Purdue University, West Lafayette, IN, USA, Dec. 1997.

[8] A. G. J. Macfarlane and I. Postlethwaite, "The generalized Nyquist stability criterion and multivariable root loci," *Int. J. Control*, vol. 25, no. 1, pp. 81–127, 1977.

[9] J. Sun, "Impedance-based stability criterion for grid-connected inverters," *IEEE Trans. Power Electron.*, vol. 26, no. 11, pp. 3075–3078, Nov. 2011.

[10] R. Burgos, D. Boroyevich, F. Wang, K. Karimi, and G. Francis, "On the ac stability of high power factor three-phase rectifiers," in *Proc. IEEE Energy Conv. Congr. Expo.*, Sep. 2010, pp. 3075–3078.

[11] S. Vesti, T. Suntio, J. A. Oliver, R. Prieto, and J. A. Cobos, "Impedance-based stability and transient-performance assessment applying maximum peak criteria," *IEEE Trans. Power Electron.*, vol. 28, no. 5, pp. 2099–2104, May 2013.

[12] M. Belkhayat, R. Cooley, and E. Abed, "Stability and dynamics of power systems with regulated converters," in *Proc. IEEE Int. Symp. Circuits Syst.*, May 1995, vol. 1, pp. 143–145.

[13] L. Harnefors, M. Bongiorno, and S. Lundberg, "Input-admittance calculation and shaping for controlled voltage-source converters," *IEEE Trans. Power Electron.*, vol. 54, no. 6, pp. 3323–3334, Dec. 2007.

[14] M. Céspedes and J. Sun, "Impedance shaping of three-phase grid-parallel voltage-source converters," in *Proc. IEEE Appl. Power Electron. Conf.*, Feb. 2012, pp. 754–760.

[15] M. Céspedes and J. Sun, "Impedance modeling and analysis of grid-connected voltage-source converters," *IEEE Trans. Power Electron.*, vol. 29, no. 3, pp. 1254–1261, Mar. 2014.

[16] J. He and Y. W. Li, "Generalized closed-loop control schemes with embedded virtual impedances for voltage source converters with LC or LCL

filters," *IEEE Trans. Power Electron.*, vol. 27, no. 4, pp. 1850–1861, Apr. 2012.
[17] J. Huang, K. Corzine, and M. Belkhayat, "Single-phase ac impedance modeling for stability of integrated power systems," in *Proc. IEEE Electric. Ship Technol. Symp.*, 2007, pp. 483–489.
[18] S. Chandrasekaran, D. Boroyevich, and D. Lindner, "Input filter interactions in three phase ac-dc converters," in *Proc. IEEE Power Electron. Spec. Conf.*, Jun. 1999, vol. 2, pp. 987–992.
[19] C. Wan, M. Huang, C. K. Tse, S. C. Wong, and X. Ruan, "Nonlinear behavior and instability in a three-phase boost rectifier connected to a non-ideal power grid with an interacting load," *IEEE Trans. Power Electron.*, vol. 28, no. 7, pp. 3255–3265, Jul. 2013.
[20] M. Huang, C. K. Tse, S. C. Wong, C. Wan, and X. Ruan, "Low-frequency Hopf bifurcation and its effects on stability margin in three-phase PFC power supplies connected to non-ideal power grid," *IEEE Trans. Circuits Syst. I, Reg. Papers*, vol. 60, no. 12, pp. 3328–3340, Dec. 2013.
[21] J. Sun, "Small-signal methods for ac distributed power systems—A review," *IEEE Trans. Power Electron.*, vol. 24, no. 11, pp. 2545–2554, Nov. 2009.
[22] L. Harnefors, M. Bongiorno , and S. Lundberg, "Input-admittance calculation and shaping for controlled voltage-source converters," *IEEE Trans. Ind. Electron.*, vol. 54, no. 6, pp. 3323–3334, Dec. 2007.
[23] R. Ni, Y. W. Li, Y. Zhang, N. R. Zargari, and Z. Cheng, "Virtual impedance-based selective harmonic compensation (VI-SHC) PWM for current source rectifiers," *IEEE Trans. Power Electron.*, vol. 29, no. 7, pp. 3346–3356, Jul. 2014.
[24] Y. Zhang, W. Xie, Z. Li, and Y. Zhang, "Model predictive direct power control of a PWM rectifier with duty cycle optimization," *IEEE Trans. Power Electron.*, vol. 28, no. 11, pp. 5343–5351, Nov. 2013.
[25] W. Zhang, Y. Hou, X. Liu, and Y. Zhou, "Switched control of three-phase voltage source PWM rectifier under a wide-range rapidly varying active load," *IEEE Trans. Power Electron.*, vol. 27, no. 2, pp. 881–890, Feb. 2012.
[26] J. Mulethaler, M. Schweizer, R. Blattmann, J. W. Kolar, and A. Ecklebe, "Optimal design of LCL harmonic filters for three-phase PFC rectifiers," *IEEE Trans. Power Electron.*, vol. 28, no. 7, pp. 3114–3125, Jul. 2013.
[27] Z. Süto and I. Nagy, "Analysis of nonlinear phenomena and design aspects of three-phase space-vector-modulated converters," *IEEE Trans. Circuits Syst. I, Fundam. Theory Appl.*, vol. 50, no. 8, pp. 1064–1071, Aug. 2003.
[28] D. Dai, S. Li, X. Ma, and C. K. Tse, "Slow-scale instability of single-stage power-factor-correction power supplies," *IEEE Trans. Circuits Syst. I, Fundam. Theory Appl.*, vol. 54, no. 8, pp. 1724–1735, Aug. 2007.
[29] X. Xiong, C. K. Tse, and X. Ruan, "Bifurcation analysis of standalone photovoltaic-battery hybrid power system," *IEEE Trans. Circuits Syst. I, Reg. Papers*, vol. 60, no. 5, pp. 1354–1365, May. 2013.
[30] Qi Wu and S. Wang, *Principles of Automatic Control*. Beijing, China: Tsinghua Univ. Press, 2010.
[31] E. Rodriguez, A. El Aroudi, F. Guinjoan, and E. Alarcon, "A ripple-based design-oriented approach for predicting fast-scale instability in DC-DC switching power supplies," *IEEE Trans. Circuits Syst. I , Reg. Paper*, vol. 59, no. 1, pp. 215–227, Jan. 2012.
[32] C. K. Tse, *Complex Behavior of Switching Power Converters*. Boca Raton, FL, USA: CRC Press, 2003.
[33] C. K. Tse and M. Li, "Design-oriented bifurcation analysis of power electronics systems," *Int. J. Bifurcation Chaos*, vol. 21, no. 6, pp. 1523–1539, Jun. 2011.

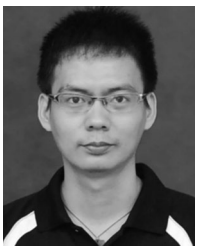

Cheng Wan received the B.S. degree in hydraulic and hydropower engineering from Wuhan University, Wuhan, China, in 2009, and the Ph.D. degree in electrical and electronic engineering from the Huazhong University of Science and Technology, Wuhan, in 2014.

He is currently an Engineer with United Imaging Healthcare Ltd., Shanghai, China, specializing in the design of gradient power amplifiers for magnetic resonance imaging applications. His research interests include power electronics, renewable energy systems, nonlinear control and applications.

Meng Huang (S'11–M'13) received the B.Eng. and M.Eng. degrees in electronic science and technology from the Huazhong University of Science and Technology, Wuhan, China, in 2006 and 2008, respectively, and the Ph.D. degree from the Hong Kong Polytechnic University, Hong Kong, in 2013. His Ph.D. thesis topic is on nonlinear analysis of grid-connected power converters.

He joined the School of Electronic Engineering, Wuhan University, Wuhan, as a Lecturer in 2013. His research interests include power electronics, nonlinear analysis and applications.

Chi K. Tse (M'90–SM'97–F'06) received the B.Eng. (Hons.) degree in electrical engineering and the Ph.D. degree from the University of Melbourne, Melbourne, Australia, in 1987 and 1991, respectively.

He is currently a Chair Professor of electronic engineering at the Hong Kong Polytechnic University, Hong Kong. From 2005 to 2012, he was the Head of Department of Electronic and Information Engineering at the same university. His research interests include complex network applications, power electronics and nonlinear systems.

Dr. Tse serves as an Editor-in-Chief for the IEEE CIRCUITS AND SYSTEMS MAGAZINE and the IEEE CIRCUITS AND SYSTEMS SOCIETY NEWSLETTER. He was/is an Associate Editor for the IEEE TRANSACTIONS ON CIRCUITS AND SYSTEMS PART I—FUNDAMENTAL THEORY AND APPLICATIONS from 1999 to 2001 and again from 2007 to 2009. He has also been an Associate Editor for the IEEE TRANSACTIONS ON POWER ELECTRONICS since 1999. He is on the Editorial Board of the *International Journal of Circuit Theory and Applications* and the *International Journal and Bifurcation and Chaos.* He received the Best Paper Award from the IEEE TRANSACTIONS ON POWER ELECTRONICS in 2001 and the Best Paper Award from the *International Journal of Circuit Theory and Applications* in 2003. In 2005 and 2011, he was selected and appointed as the IEEE Distinguished Lecturer. In 2007, he received the Distinguished International Research Fellowship by the University of Calgary, Canada. In 2009 and 2013, he and his coinventors received the Gold Medal at the International Exhibition of Inventions of Geneva, Switzerland, on LED lighting technologies. In 2011, he was appointed as an Honorary Professor by RMIT University, Melbourne. In 2013, he received the Gledden Fellowship by the University of Western Australia, Perth, Australia.

Xinbo Ruan (M'97–SM'02) was born in Hubei, China, in 1970. He received the B.S. and Ph.D. degrees in electrical engineering from the Nanjing University of Aeronautics and Astronautics (NUAA), Nanjing, China, in 1991 and 1996, respectively.

In 1996, he joined the Faculty of Electrical Engineering Teaching and Research Division, NUAA, where he became a Professor in the College of Automation Engineering in 2002 and has been involved in teaching and research in the field of power electronics. From August to October 2007, he was a Research Fellow in the Department of Electronic and Information Engineering, Hong Kong Polytechnic University, Hong Kong. Since March 2008, he has been also with the College of Electrical and Electronic Engineering, Huazhong University of Science and Technology, Wuhan, China. He is a Guest Professor with Beijing Jiaotong University, Beijing, China, Hefei University of Technology, Hefei, China, and Wuhan University, Wuhan. He is the author or coauthor of four books and more than 100 technical papers published in journals and conferences. His main research interests include soft-switching dc–dc converters, soft-switching inverters, power factor correction converters, modeling the converters, power electronics system integration, and renewable energy generation system.

Dr. Ruan received the Delta Scholarship by the Delta Environment and Education Fund in 2003 and a Special Appointed Professor of the Chang Jiang Scholars Program by the Ministry of Education, China, in 2007. Since 2005, he has been serving as a Vice President of the China Power Supply Society, and since 2008, he has been a Member of the Technical Committee on Renewable Energy Systems within the IEEE Industrial Electronics Society. He has been an Associate Editor for the IEEE TRANSACTIONS ON INDUSTRIAL ELECTRONICS and the IEEE JOURNAL OF EMERGING AND SELECTED TOPICS ON POWER ELECTRONICS since 2011 and 2013, respectively. He is a Senior Member of the IEEE Power Electronics Society and the IEEE Industrial Electronics Society.